Disorder-induced Raman scattering in rhenium trioxide (ReO$_3$)

Disorder-induced Raman scattering in rhenium trioxide (ReO$_3$)

J Purans[1,2], A Kuzmin[2], E Cazzanelli[3] and G Mariotto[1]

[1] Dipartimento di Fisica, Università di Trento, I-38050 Povo (Trento), Italy
[2] Institute of Solid State Physics, University of Latvia, Kengaraga street 8, LV-1063 Riga, Latvia
[3] LICRYL-CNR and CEMIF.CAL, Dipartimento di Fisica, Università della Calabria, I-87036 Arcavacata di Rende (Cosenza), Italy

E-mail: xas@latnet.lv (J Purans) and a.kuzmin@cfi.lu.lv

Abstract
Raman scattering in cubic metallic perovskite (ReO$_3$) was studied at room temperature for well-crystallized monolith, polycrystalline powder and thin film samples. Defect-induced first-order Raman scattering was detected from the sub-surface region, given by the penetration depth of a 633 nm laser, and its origin was explained on the basis of a rigid-ion vibrational model for bulk ReO$_3$. A quenching of the Raman intensity was observed in crystalline monolithic ReO$_3$ upon increasing the temperature up to 250 °C and was related to crystal surface reconstruction/annealing.

1. Introduction

Transition metal oxides (TMOs) constitute a very interesting class of materials because of the variety of functional properties and phenomena exhibited by them. Among different TMOs, rhenium trioxide (ReO$_3$) [1] is known for its unexpectedly high electrical conductivity similar to that of copper, therefore it is often referred as a 'covalent metal' [2–5]. ReO$_3$ is also unusual in that the cubic perovskite-type structure (ABO$_3$) is non-distorted at atmospheric pressure at all temperatures [1, 6]. The empty A sites permit wide librational motions of the ReO$_6$ octahedra, resulting in an enhanced compressibility and ultra low or negative thermal expansion [7]. In contrast to ReO$_3$, tungsten trioxide WO$_3$ as well as many perovskites, like SrTiO$_3$, BaTiO$_3$ and KNbO$_3$, show the condensation of one or more optical modes causing the rearrangement of the local electronic and atomic structure and related structural phase transitions [8].

In spite of the fact that cubic ReO$_3$ is widely used as a model of an ideal perovskite structure, only a few theoretical works have so far been devoted to the investigation of its vibrational properties [9–11]. The common feature for all previous works is the prediction of high-frequency modes occurring at the Brillouin zone centre (Γ point) at 700–1000 cm^{-1}

[9–11]. Besides, a gap in the phonon density of states (PDOS) was predicted to be between 500 and 900 cm^{-1} in [9] and between 600 and 800 cm^{-1} in [10].

A factor group analysis for cubic ReO_3 predicts 12 normal modes of vibration, which correspond to the following irreducible representation at the Brillouin zone centre, $\Gamma_{O_h^1} = 2F_{1u}(IR) + F_{2u} + F_{1u}(acoustic)$, where two $F_{1u}(IR)$ are infrared (IR) active ungerade optic modes, F_{2u} is a 'silent' mode, and $F_{1u}(acoustic)$ corresponds to an acoustic mode. Since no gerade optic modes are predicted, no Raman signal is expected for perfect cubic ReO_3.

Unfortunately, the experimental results published on vibrational properties of cubic ReO_3 are controversial enough. To our knowledge, only one experimental paper has been published up to now on the infrared and Raman spectroscopy of ReO_3 [9]: two bands at 315 and 905 cm^{-1} have been reported in the IR spectrum of a thin film produced by thermal evaporation of ReO_3 powder, while a set of bands between 200 and 2000 cm^{-1} has been observed in the Raman spectrum from single-crystal ReO_3, and the bands at 600, 1220 and 1820 cm^{-1} have been attributed to second-order Raman scattering. Note that our results discussed below do not reproduce the Raman spectrum reported in [9].

In this work, we report on the results of a Raman scattering study of ReO_3 in the form of a well-crystallized monolith, polycrystalline powder and thin films, and discuss the origin of the Raman bands on the basis of the rigid-ion vibrational model. The experimental work described here constitutes the first real light scattering investigation on cubic ReO_3, apart from [9], in which the serious technical difficulties posed by Raman spectroscopy of this compound have been addressed.

2. Experiment

The polycrystalline ReO_3 (99.9%) sample used was commercial powder from Metalli Preziosi SpA. It had a red colour, and its quality was checked by x-ray powder diffraction. This powder was used as a starting material for producing several other samples. Some quantity of ReO_3 powder was ground by hand in an agate mortar for variable times, up to 10 min. Thin films can be easily obtained by simple evaporation of ReO_3 powder, in open air, when the temperature is in the range 200–250 °C, since strong sublimation of ReO_3 occurs above 200 °C. The films of ReO_3 were deposited on the silica window of a small optical oven by heating the ReO_3 powder above 200 °C, while the window, located at about 1 cm above the hot finger, was at room temperature. Such films have also been deposited by evaporation of the ReO_3 powder on clean and ITO-coated glasses, located a few centimetres above, inside a large oven at a constant temperature of 210 °C for variable lengths of time. Finally, a well-crystallized red-coloured ReO_3 monolith, having a size of about 7 μm × 4 μm, was selected under an optical microscope from virgin powder.

The Raman measurements were performed by a Raman microprobe set-up (HORIBA Jobin Yvon, model Labram). A He–Ne laser (632.8 nm emission) was used as the excitation source. The collection optics was a 50× Mplan Olympus long working distance objective. The power of the laser out of the objective was about 5 mW and the focused laser spot had about 2–3 μm of apparent diameter. To avoid heating the samples, the spectra were excited by a reduced laser power obtained by using filters with optical density (OD) 2 or 1. The experimental resolution of about 2 cm^{-1} was achieved with a 1800 grooves mm^{-1} grating. Powder samples were just spread on a standard glass microscope slide, or, in the case of temperature dependent measurements, on an aluminium foil covering the hot finger of an optical oven (Linkam model THMS 600).

The Raman spectra obtained at room temperature for different ReO_3 specimens are shown in figure 1. Figure 2 shows the temperature evolution of Raman scattering from the monolithic
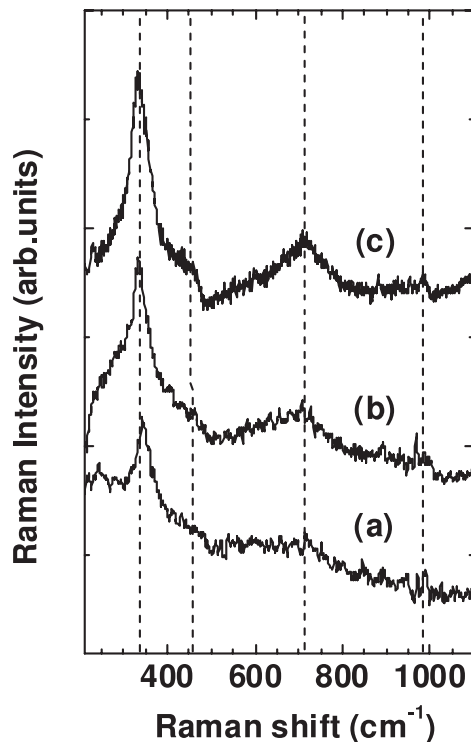
Figure 1. Room temperature Raman scattering in ReO$_3$: (a) monolith, (b) polycrystalline powder and (c) thin film.

sample. Finally, the spectral effects of grinding on polycrystalline ReO$_3$ are illustrated in figure 3.

3. Results and discussion

3.1. Raman spectroscopy

Room temperature Raman spectra of ReO$_3$ in the form of a well-crystallized monolith, polycrystalline powder and evaporated thin film are similar, despite the fact that the spectral intensity becomes more pronounced on passing from the monolith to the film (figure 1). This suggests a similar origin for the Raman scattering in each sample.

The Raman spectrum of ReO$_3$ consists of two main bands at ∼336 and ∼720 cm^{-1} and a less defined band at ∼447 cm^{-1}. There is also some evidence of a broad and very weak band at 850–1000 cm^{-1}, more visible in the powder and thin film samples. Note that our Raman spectra from ReO$_3$ differ from those previously published in [9].

We attribute the observed bands to first-order Raman scattering in a sub-surface region of ReO$_3$, having a thickness in the range 10–20 nm as estimated from the penetration depth of our laser in metallic ReO$_3$, calculated using Maxwell's equations and the resistivity value of ReO$_3$ [3] at room temperature. Due to the $\Delta k = 0$ selection rule, the first-order Raman scattering in a bulk crystal probes optical phonons at the centre (Γ-point) of the Brillouin zone. However, the small penetration depth of the laser light in comparison with its wavelength leads to the softening of this selection rule. Therefore, a broader interval in k-space around
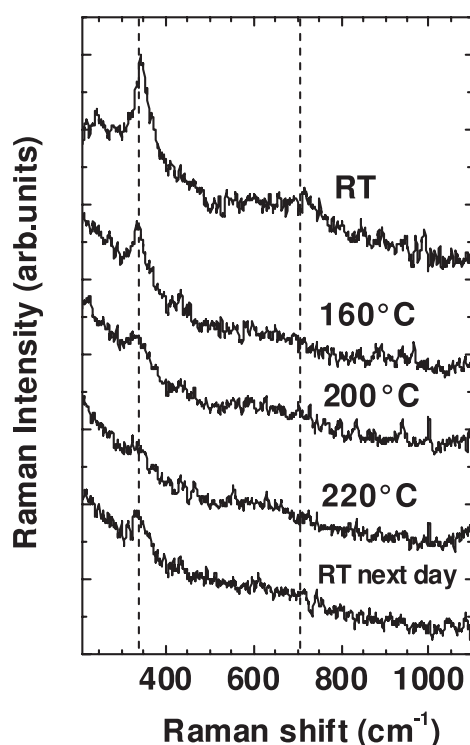
3

Figure 2. Temperature dependence of the Raman scattering in monolithic ReO_3.

the Γ-point affects the frequency distribution of the scattered light, with the frequencies near the Γ-point producing the strongest contribution. As a result, the observed Raman spectra (figure 1) consist of rather broad bands. Besides, the stress and/or the presence of native crystal defects can induce local symmetry lowering and thus contribute to an increase in the scattering intensity. Such an interpretation correlates well with the intensity of the Raman signals, this being largest in the thin film.

The influence of native crystal defects can be significantly reduced at high temperatures. The temperature dependence of the Raman spectrum in the well-crystallized ReO_3 monolith (figure 2) results in the remarkable quenching of its intensity on heating above 200 °C, and such a decrease in intensity seems to be stable, at least for times of the order of days. Since this temperature is a starting point for ReO_3 evaporation, which was also used in the preparation of our thin films, one can explain the observed Raman behaviour by the process of crystal surface reconstruction/annealing upon evaporation. It is interesting to note that a reduction in the hydrogen content of ReO_3, together with the connected structural deformation [12], also occurs when rhenium oxide crystals reach temperatures in the range of 220–230 °C.

One should also note that the ReO_3 fresh surface seems to have a strong reactivity, henceforth a catalytic activity with respect to dissociation of atmospheric compounds, like CO_2 and H_2O. The former case could be correlated to the Raman spectroscopic evidence for amorphous carbon formation, as discussed elsewhere [13], while the second dissociation reaction can explain the number of hydrogen impurities trapped in the sub-surface layers [12].

A different type of surface defect in ReO_3 can be produced by grinding the polycrystalline powder (figure 3). In these samples, a set of narrow bands appears at both low (243, 345,
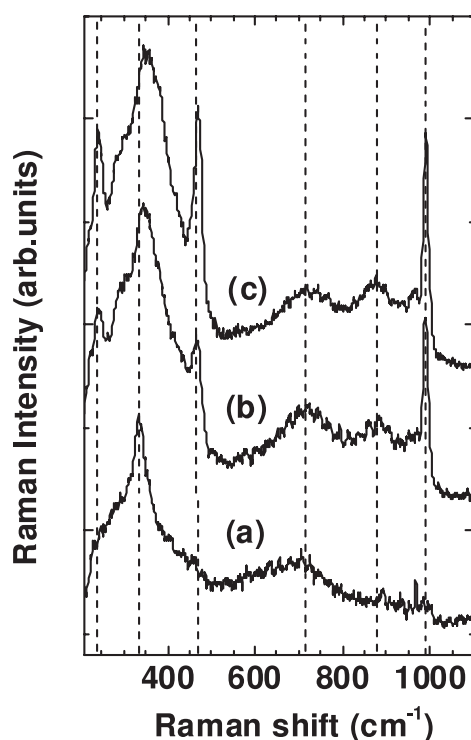
4

Figure 3. Effect of grinding on the Raman scattering in polycrystalline ReO_3: (a) fresh ground powder, (b) 2 min of grinding, (c) 10 min of grinding.

466 cm^{-1}) and high (880 and 990 cm^{-1}) frequencies. These bands can be attributed to the ReO_4 groups formed at the fresh ReO_3 surfaces exposed to air. In particular, the low-frequency modes are due to bending motion of interconnected pairs of ReO_4–ReO_4 tetrahedra, whereas the high-frequency mode at 880 cm^{-1} is due to the Re–O stretching vibration for oxygen ions shared between ReO_4 tetrahedra and ReO_6 octahedra, and the mode at 990 cm^{-1} is due to the Re–O stretching vibration in ReO_4 tetrahedra. In fact, similar vibrational modes were observed previously from various solid perrhenates and from the perrhenate ReO_4^- ion in aqueous solution [14, 15].

3.2. Lattice dynamics calculation

To interpret the origin of the Raman bands in figure 1, we performed simulations using the rigid-ion vibrational model within the quasiharmonic approximation as implemented in the GULP code [16, 17]. Since the probed sub-surface region is rather thick, the calculations were done for bulk stoichiometric ReO_3.

The short-range pairwise interactions Re–O and O–O were described by the Buckingham potential $U(r) = A \exp(-r/\rho) - Cr^{-6}$ acting over the range of 0–10 Å. The long-range Coulomb interactions were evaluated using the Ewald summation method [18] with two *effective charges* of rhenium (Z_{Re}) and oxygen (Z_O) ions. The requirement of charge neutrality imposes that $Z_{Re} + 3Z_O = 0$. For a fixed value of charges (Z_{Re} and Z_O), the parameters A, ρ and C of the Buckingham potentials were determined by fitting the experimental values of the lattice parameter $a_0 = 3.7504$ Å [1] and elastic constants $C_{11} = 5.72 \times 10^{12}$ dyn cm^{-2},
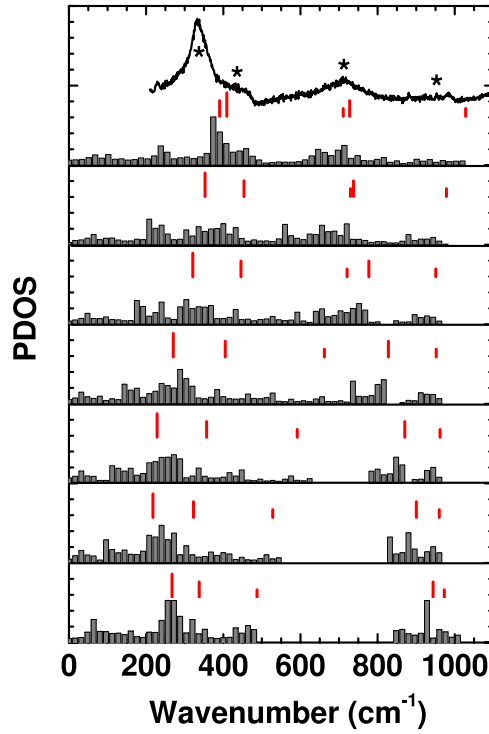
Figure 4. Comparison of the experimental Raman signal of ReO_3 (upper curve) and phonon density of states (PDOS), calculated for different charge values Z_{Re}: 6.0, 5.49, 5.04, 4.50, 3.99, 3.39 and 2.7 (from top to bottom). The positions of $k = 0$ phonon modes are indicated for each Z_{Re} by vertical lines above the corresponding PDOS. The main features in the experimental spectrum are labelled by asterisks.

(This figure is in colour only in the electronic version)

$C_{12} = 0.07 \times 10^{12}$ dyn cm^{-2} and $C_{44} = 0.68 \times 10^{12}$ dyn cm^{-2} [19] using the free energy minimization and 'relaxed' fitting techniques [17]. After optimization of the interatomic potentials, the phonon dispersion curves and densities were calculated by integration on a $20 \times 20 \times 20$ grid of equidistant irreducible k-points across the first Brillouin zone using the Monkhorst–Pack method [20]. The full procedure was repeated several times for different values of effective charge Z_{Re} in the range between 2.7 and 6.0. Note that a variation of the effective charge from the formal one simulates the degree of covalency of the Re–O bonds.

The dependence of the PDOS and $k = 0$ phonon modes on the effective charge of the rhenium ion Z_{Re} is presented in figure 4. Qualitative comparison of calculated PDOS and $k = 0$ phonon modes with the experimental Raman spectrum at room temperature allows us to conclude that the best agreement between $k = 0$ modes and the bands position in the experimental Raman spectra is observed for $Z_{Re} \approx 5.49$. The corresponding set of interatomic potential parameters and dispersion curves for $Z_{Re} = 5.49$ is reported in table 1 and in figure 5, respectively.

We will now compare the results of the theoretical lattice dynamics calculations for ReO_3 from [9–11] with our calculations and experimental Raman spectra. Since all three of our samples show similarly shaped Raman spectra, but the thin film has the most pronounced bands, its Raman signal is used in the comparison in figure 4.
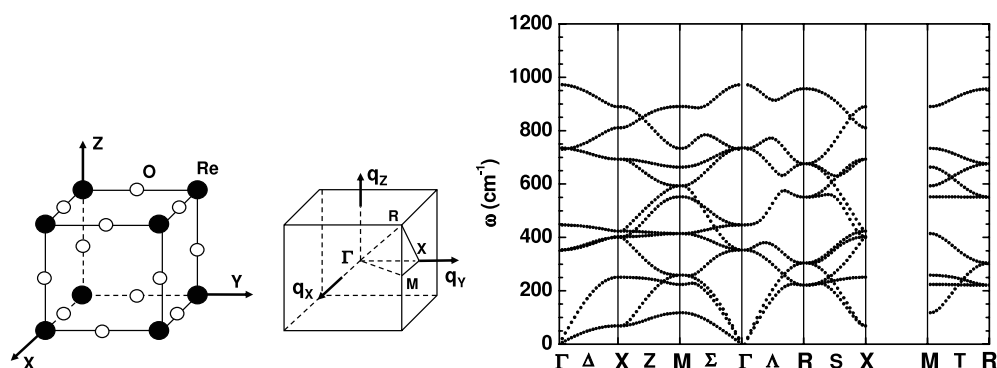
Figure 5. Crystal structure, the first Brillouin zone and phonon dispersion curves ($Z_{Re} = 5.49$) for cubic ReO_3.

Table 1. Parameters of the Buckingham and Coulomb potentials, used in the calculation of the dispersion curves for ReO_3 in figure 1. The calculated lattice parameter is 3.748 Å.

Pair of atoms	A (eV)	ρ (Å)	C (eV Å^{-6})
Re–O	992.219	0.389 519	0.0
O–O	84 652.4	0.075 667	32.0

Atoms	Z (e)		
Re	5.49		
O	−1.83		

Until now the optical phonons at the Brillouin zone centre (Γ-point) in ReO_3 have been experimentally observed only by IR transmission spectroscopy in thin film and fine powder [9]. The two bands, found at room temperature at 315 and 905 cm^{-1} [9], were assigned to the IR active bending O–Re–O and stretching Re–O modes, respectively. Using a simple valence force field model, the three force constants, describing the two (bending and stretching) interactions and the repulsion force between the nearest oxygen atoms, were evaluated from three elastic constants [9]. Based on the thus obtained force constants, the authors of [9] estimated the IR frequencies to be 354 and 991 cm^{-1} and approximately evaluated the phonon dispersion curves: these indicated a large separation of about 500 cm^{-1} between the high-frequency modes and other modes for all directions in the Brillouin zone.

Later, more accurate theoretical calculations [10] were performed within the rigid-ion model, taking into account nearest neighbour (Re–O and O–O) and electrostatic interactions. The four force constants and the effective charge of the oxygen ion ($Z_{Re} = -3Z_O$) were fitted to the known values of free elastic constants and two IR frequencies. The obtained results confirmed the existence of a gap of about 200 cm^{-1} between ∼600 and ∼800 cm^{-1} in the ReO_3 one-phonon DOS [10].

In a recent first-principles study of ReO_3 [11], the presence of high-frequency stretching modes at 760–822 cm^{-1} was confirmed and the position of the bending modes at about 433–438 cm^{-1} was estimated. However, no calculation of the phonon dispersion curves was made in [11], so we cannot discuss the existence of the gap.

Looking at our experimental Raman spectra (figure 1), one can see that there is a band maximum at 720 cm^{-1}, being roughly in the middle of the predicted gap [9, 10]. To account for this discrepancy, the PDOS for the effective charges of several rhenium ions are shown

7

in figure 4. We found that the appearance and the width of the gap depend strongly on the effective charge of the rhenium ions Z_{Re}, and the gap exists for $Z_{Re} < 3.39$. In particular, the case of $Z_{Re} = 3.39$ corresponds to that in [10], whereas a value of $Z_{Re} = 5.49$ gives the best agreement between $k = 0$ modes and the bands position in our experimental Raman spectra.

4. Conclusions

The Raman spectra of ReO_3 in the form of a well-crystallized monolith, polycrystalline powder and thin film were analysed. First-order Raman scattering was observed from the sub-surface region of 10–20 nm thickness and explained on the basis of a rigid-ion vibrational model for bulk ReO_3. We found that the effective charge of rhenium ions plays an important role and is responsible for the absence of the gap in PDOS, whose existence was previously proposed in [9, 10]. We also observed that an increase in temperature to 250 °C quenches the Raman intensity. Finally, the activity of a fresh ReO_3 surface in air leads to the appearance of new Raman bands related to the presence of the surface species.

Acknowledgments

References

[1] Jørgensen J E, Jørgensen J D, Batlogg B, Remeika J P and Axe J D 1986 *Phys. Rev.* B **33** 4793
[2] Allen P B and Schulz W W 1993 *Phys. Rev.* B **47** 14434
[3] Pearsall T P and Lee C A 1974 *Phys. Rev.* B **10** 2190
[4] King C N, Kirsch H C and Geballe T H 1971 *Solid State Commun.* **9** 907
[5] Tanaka T, Akahane T, Bannai E, Kawai S, Tsuda N and Ishizawa Y 1976 *J. Phys. C: Solid State Phys.* **9** 1235
[6] Chang T S and Trucano P 1978 *J. Appl. Crystallogr.* **11** 286
[7] Tao J Z and Sleight A W 2003 *J. Solid State Chem.* **173** 442
[8] Goodenough J B 1966 *J. Appl. Phys.* **37** 1415
     Goodenough J B 1971 *Prog. Solid State Chem.* **5** 145
[9] Ishii M, Tanaka T, Akahana T and Tsuda N 1976 *J. Phys. Soc. Japan* **41** 908
[10] Gabrusenok E V 1983 *Izv. Akad. Nauk Latv. SSR Ser. Fiz. Tech. Nauk.* **1** 66
[11] Stachiotti M G, Corà F, Catlow C R A and Rodriguez C O 1997 *Phys. Rev.* B **55** 7508
[12] Horiuchi S, Kimizuka N and Yamamoto A 1979 *Nature* **279** 226
[13] Cazzanelli E, Castriota M, Marino S, Scaramuzza N, Purans J, Kuzmin A, Kalendarev R, Mariotto G and
     Das G 2007 *Sol. Energy Mater. Sol. Cells* submitted
[14] Beattie I R and Ozin G A 1969 *J. Chem. Soc.* A 2615
[15] Hard F D, Wachs I E, Horsley J A and Via G H 1988 *J. Mol. Catal.* **46** 15
[16] Gale J D 1996 *Phil. Mag.* B **73** 3
[17] Gale J D and Rohl A L 2003 *Mol. Simul.* **29** 291
[18] Ewald P P 1921 *Ann. Phys.* **64** 253
[19] Tsuda N, Sumino Y, Ohno I and Akahane T 1976 *J. Phys. Soc. Japan* **41** 1153
[20] Monkhorst H J and Pack J D 1976 *Phys. Rev.* B **13** 5188